

## Plasmonic-induced transparency of unsymmetrical grooves shaped metal–insulator–metal waveguide

Jicheng Wang, Lin Sun, Zheng-Da Hu, Xiuye Liang, and Cheng Liu

Citation: *AIP Advances* **4**, 123006 (2014); doi: 10.1063/1.4902506

View online: <http://dx.doi.org/10.1063/1.4902506>

View Table of Contents: <http://scitation.aip.org/content/aip/journal/adva/4/12?ver=pdfcov>

Published by the [AIP Publishing](#)

---

### Articles you may be interested in

**Surface plasmon coupling efficiency from nanoslit apertures to metal-insulator-metal waveguides**  
Appl. Phys. Lett. **101**, 121112 (2012); 10.1063/1.4754137

**Subwavelength slow-light waveguides based on a plasmonic analogue of electromagnetically induced transparency**  
Appl. Phys. Lett. **99**, 143117 (2011); 10.1063/1.3647951

**Thermo-optic microring resonator switching elements made of dielectric-loaded plasmonic waveguides**  
J. Appl. Phys. **109**, 073111 (2011); 10.1063/1.3564949

**Understanding the dispersion of coaxial plasmonic structures through a connection with the planar metal-insulator-metal geometry**  
Appl. Phys. Lett. **94**, 231111 (2009); 10.1063/1.3148692

**Schrödinger solitons in left-handed SiO<sub>2</sub> – Ag – SiO<sub>2</sub> and Ag – SiO<sub>2</sub> – Ag plasmonic waveguides calculated with a nonlinear transmission line approach**  
J. Appl. Phys. **104**, 124510 (2008); 10.1063/1.3048548

---



**Goodfellow**  
metals • ceramics • polymers  
composites • compounds • glasses

**Save 5% • Buy online**  
**70,000 products • Fast shipping**

# Plasmonic-induced transparency of unsymmetrical grooves shaped metal–insulator–metal waveguide

Jicheng Wang,<sup>a,b</sup> Lin Sun,<sup>b</sup> Zheng-Da Hu, Xiuye Liang, and Cheng Liu

*Department of Optoelectronic Information Science and Engineering, Jiangnan University,  
1800 Lihu Avenue, Wuxi 214122, China*

(Received 18 September 2014; accepted 3 November 2014; published online 20 November 2014)

The plasmonic waveguides with unsymmetrical grooves shaped metal-insulator-metal (MIM) structures are proposed in theory. For symmetrical and unsymmetrical groove structures, the transmission varies with the increasing of the groove depths and groove lengths. The filtering characteristics due to the destructive interference of the plasmonic modes are found in those subwavelength structures. The transmission line theory is utilized to interpret the transmittance and filtering phenomena. The transmission formulas are also achieved by the transmission line theory. It is found that the slow light effects are emerged in the unsymmetrical groove structures. A small group velocity ( $c/80$ ) can be achieved. Finite Element Method (FEM) is conducted to verify our design. © 2014 Author(s). All article content, except where otherwise noted, is licensed under a Creative Commons Attribution 3.0 Unported License. [http://dx.doi.org/10.1063/1.4902506]

## I. INTRODUCTION

Surface plasmon polaritons (SPPs), coupled modes of plasmons and photons, propagate along a metal-dielectric interface.<sup>1,2</sup> The SPPs are electromagnetic surface modes and have unique potential to guide light in a region beyond the so-called diffraction limit.<sup>3</sup> Nowadays, the SPPs have drawn more attentions in concentrating and channeling light at sub-wavelength scale, and become a strong candidate in realizing integrated optical circuits including sub-wavelength and/or nanometer-size optical devices.<sup>4</sup> Recently, a lot of devices based on SPPs, especially metal-insulator-metal (MIM) plasmonic waveguide, have been investigated both theoretically and experimentally, such as splitters,<sup>5</sup> U-shaped waveguides,<sup>6</sup> Y-shaped combiners,<sup>7</sup> couplers,<sup>8</sup> multimode-interferometers,<sup>9</sup> and Mach-Zehnder interferometers.<sup>10</sup> Above these structures, MIM waveguides have attracted much attention for the better confinement of light with an acceptable propagation length for surface plasmon polaritons (SPPs).<sup>11,12</sup> The device with asymmetrical nanostructures on both sides of the nanoslit, which is capable of confining and guiding light waves, was proposed by Gan.<sup>13</sup> Based on plasmonic Bragg grating structure, Gan also discussed bidirectional splitters for SPPs in THz and near infrared, respectively.<sup>14,15</sup> Using the similar gratings-based metallic structure, Bonod achieved unidirectional control of SPPs.<sup>16</sup> Tejeira demonstrated a unidirectional nanoslit coupler by placing nanogrooves on one side of the nanoslit to focus light on a chosen location, theoretically and experimentally.<sup>17</sup>

When a light pulse propagates in a dispersive medium, light velocity is affected by the frequency dependence of the refractive index. The slow or even stopped light can be achieved. Slow light allows for exciting new possibilities in the fields of all-optical processing,<sup>18</sup> information storage,<sup>19</sup> optical memory,<sup>20</sup> nonlinear optics<sup>21</sup> and optical buffers.<sup>22</sup> In general, there are many approaches to generate slow light, such as quantum interference effects or electromagnetically induced transparency (EIT). EIT is a quantum phenomenon that observed in three-level atomic systems due to the quantum interference.<sup>23</sup> It features strong dispersion and slow-light propagation within the

<sup>a</sup>Corresponding author: jcwang@jiangnan.edu.cn

<sup>b</sup>These authors contributed equally to this work.

transparency window.<sup>24</sup> Recently, it has been demonstrated that EIT-like spectrum can be realized in classical configurations, such as coupled dielectric resonators,<sup>25</sup> acoustic analogy of the EIT effect,<sup>26</sup> phase-coupled plasmonic-induced transparency,<sup>27</sup> and plasmonic-induced transparency (PIT) in metal-dielectric-metal waveguide bends.<sup>28</sup> PIT is the counterpart of the EIT effect in plasmonics systems, which is widely investigated, because “light slowing” elements with subwavelength sizes or metamaterials can be achieved.<sup>29–38</sup>

In this paper, the metal-insulator-metal (MIM) plasmonic waveguides with unsymmetrical groove structures are proposed. By changing the depths and the lengths of the groove structures, the transmission of SPPs can be adjusted, and filtering characteristics are found in both the symmetrical and unsymmetrical structures. The filter frequencies are related to the depths and lengths of the groove structures. Based on the transmission line theory, the transmittance formulas of those structures can be achieved. The transmittance curves with the different wavelengths are considered. From those curves, we can demonstrate that the transmission of the proposed structures can be modulated by altering the depths and the lengths of the structures. Attributing to the SPPs constructive interference, this structure possesses high transmission. In addition, the slow light effect is found in the unsymmetrical groove structures. Analytical and numerical results on slow light in unsymmetrical groove structures are proposed.

## II. MODEL AND NUMERICAL METHOD

In the MIM plasmon waveguide, the metal is assumed as silver whose frequency-dependent complex relative permittivity is characterized by the Drude model,

$$\varepsilon_m(\omega) = \varepsilon_\infty - \frac{\omega_p^2}{\omega^2 + i\gamma\omega}. \quad (1)$$

Here,  $\omega_p = 9.1\text{eV}$  stands for the bulk plasma frequency which represents the natural frequency of the oscillations of free conduction electrons.  $\gamma = 0.018\text{eV}$  is the damping frequency of the oscillations.  $\varepsilon_\infty = 3.7$  is the Ag dielectric constant at infinite angular frequency. The dielectric constant of air is 1.  $\omega$  is the angular frequency of the incident light. A TM-polarized plane wave is used to excite the SPPs.

Since the width of the MIM waveguide is much smaller than the incident wavelength, the MIM waveguide only supports the fundamental  $\text{TM}_0$  mode. According to the Maxwell equations and boundary conditions, the dispersion equations of the fundamental  $\text{TM}_0$  mode in the MIM waveguide can be obtained as following formula,

$$k_d\varepsilon_m + k_m\varepsilon_d \coth\left(-\frac{ik_d}{2}\omega\right) = 0. \quad (2)$$

Here,  $k_d$  and  $k_m$  defined by the momentum conservation,

$$k_d = \sqrt{\varepsilon_m k_0^2 - \beta^2}, \quad (3)$$

$$k_m = \sqrt{\varepsilon_d k_0^2 - \beta^2}. \quad (4)$$

Here,  $\varepsilon_d$  and  $\varepsilon_m$  are the dielectric constants of the insulator and metal, respectively.  $k_0 = 2\pi/\lambda_0$  is the wave vector in vacuum,  $k_d$  and  $k_m$  are the transverse propagation constants of dielectric and metal, respectively. The effective refractive index  $n_{\text{eff}} = \beta/k_0$  can be calculated by equation (2)–(4). The real part of  $n_{\text{eff}}$  in the MIM waveguide as a function of the gap width  $w$  and incident wavelength  $\lambda$  is shown in Figure 1. In Fig. 1 the metal is Ag and the insulator is air. The real part of  $n_{\text{eff}}$  decreases with the increasing of the gap width  $w$  at the same wavelength. When the gap width  $w$  is fixed,  $n_{\text{eff}}$  will be nearly unchanged with the alteration of the incident light wavelength.

We start the discussion of filtering properties of plasmonic waveguide structure with the two grooves. Fig. 2(a) shows the two symmetrical grooves model, dark component represents Ag and light component represents air. The waveguide is divided into three parts, which are gap  $A_1$ , groove  $B$ , and gap  $A_2$ .  $d_A$  and  $d_B$  are the depths of gap  $A_1$  (the same with  $A_2$ ) and groove  $B$ , respectively.  $l_A$

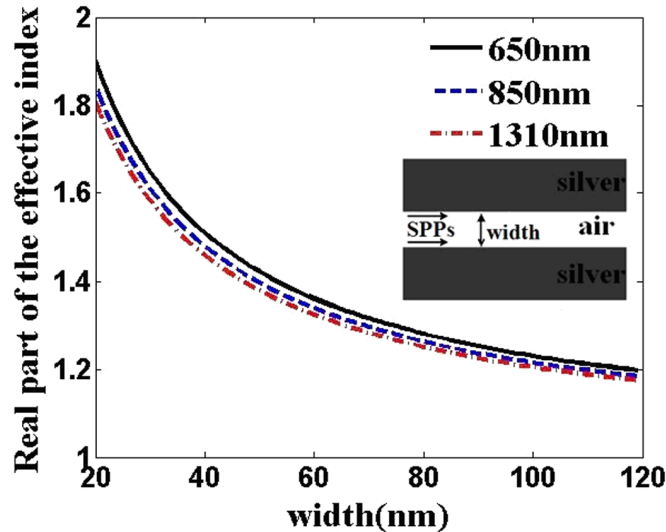


FIG. 1. Real part of the effective refractive index  $n_{\text{eff}}$  versus the wavelength  $\lambda$  under the different groove widths.

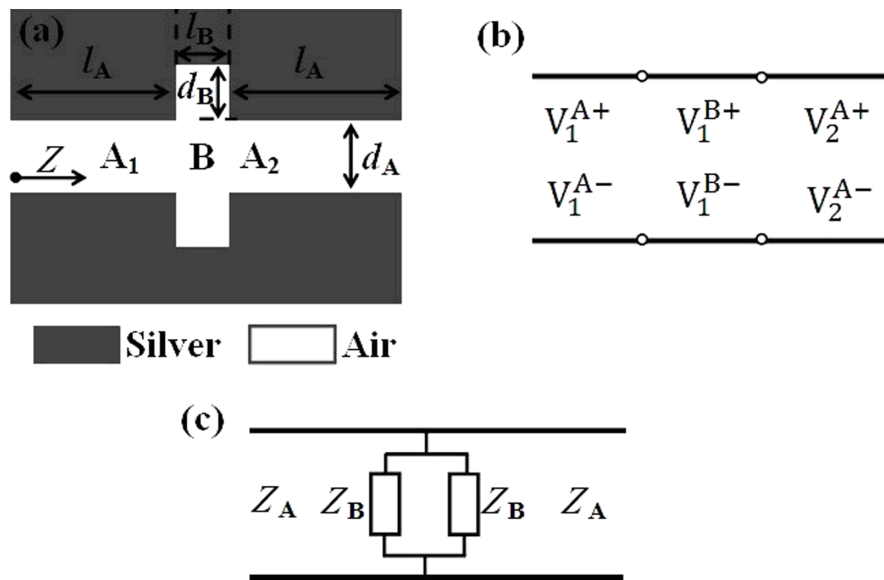


FIG. 2. (a) Schematic diagram of the symmetrical double-groove shaped plasmonic waveguide optical filters, (b) the transmission line mode of the double-groove structure, (c) the equivalent circuit of the double-groove structure.

and  $l_B$  are the lengths of gap  $A_1$  (the same with  $A_2$ ) and groove  $B$ , respectively. Here,  $l_A$  is fixed to be 100nm, and  $d_A$  is a determined value of 50nm. The TM-polarized Gaussian beam is launched along the  $z$  axis, and SPPs mode can be excited by means of end-fire coupling. The calculated area was divided by Yee's mesh with a size of 2nm. The FEM with perfectly matched layer (PML) absorbing boundary condition is employed to investigate the transmission characteristics of the structure. The transmission line mode of the symmetrical double-groove structure is shown in Fig. 2(b), and the equivalent circuit of the symmetrical double-groove structure is shown in Fig. 2(c). If the width of metal waveguide is much smaller than the wavelength, the waveguide can be approximated as the transmission line. The electromagnetic transmission in the connection of the metal waveguides can be converted to the relationship between the current and the voltage by the theory of the transmission line. The total voltage can be regarded as the incident wave voltage  $V^+$  and the reflected wave

voltage  $V^-$ . The voltage in both sides of the transmission line connection should be equal, that is,

$$V_1^+ + V_1^- = V_2^+ + V_2^- \quad (5)$$

Likewise, the total current in the transmission line can be regarded as the incident wave current  $I^+$  and the reflected wave current  $I^-$ , that is,

$$I_1^+ + I_1^- = I_2^+ + I_2^- \quad (6)$$

Here, the symbol “+” and “-” are represented as the transmission voltage (or current) that towards and backwards to the connection point, respectively. The subscript 1 and 2 are represented as gap  $A_1$  and gap  $A_2$  in the waveguide (as shown in Fig. 2(a), respectively. For TM<sub>0</sub> mode of sub-wavelength waveguide within optical frequency range, the characteristic impedance  $Z$  can be defined as the equivalent voltage and equivalent current ratio,

$$Z \equiv V/I = \frac{E_x d}{H_z h} = \frac{\beta_{re} d}{n^2 \omega \epsilon_0 h} \quad (7)$$

Here,  $\omega$  is the angular frequency of the incident light,  $h$  is the waveguide width in the  $z$  direction, and is fixed 10 μm.  $d$  is the depth of the waveguide.  $\beta_{re}$  is the real part of the propagation constant  $\beta$  for TM<sub>0</sub> mode, and the effective refractive index  $n_{eff} = \beta/k_0$ ,  $k_0 = 2\pi/\lambda_0$  is the wave vector in vacuum.  $n$  is the refractive index of insulation layer in the waveguide.

The phenomenon above can be physically explained in the Transmission-line Matrix (TML). The equivalent voltage in a waveguide can be expressed as,

$$V^A = V^{A+} e^{j\beta_A x} + V^{A-} e^{-j\beta_A x}, \quad (8)$$

$$V^B = V^{B+} e^{j\beta_B x} + V^{B-} e^{-j\beta_B x}. \quad (9)$$

Here,  $\beta_A$  and  $\beta_B$  are propagation constants for TM<sub>0</sub> mode in the waveguide gap  $A_1$  (the same with  $A_2$ ) and groove  $B$ , respectively. The symbol “+” and “-” are represented as the shaft direction and reverse direction of  $x$  axis. Using the TML formulas, one can be obtained,

$$\begin{bmatrix} V_1^+ \\ V_1^- \end{bmatrix} = D_{AB} P_B D_{BA} P_A \begin{bmatrix} V_2^+ \\ V_2^- \end{bmatrix}. \quad (10)$$

Here,  $D_{AB}$  and  $D_{BA}$  are the transmission matrixes of  $AB$  waveguide junctions as following matrixes,

$$D_{AB} = \begin{bmatrix} \frac{1}{2}(1 + \frac{Z_A}{Z_B}) & \frac{1}{2}(1 - \frac{Z_A}{Z_B}) \\ \frac{1}{2}(1 - \frac{Z_A}{Z_B}) & \frac{1}{2}(1 + \frac{Z_A}{Z_B}) \end{bmatrix}, \quad D_{BA} = \begin{bmatrix} \frac{1}{2}(1 + \frac{Z_B}{Z_A}) & \frac{1}{2}(1 - \frac{Z_B}{Z_A}) \\ \frac{1}{2}(1 - \frac{Z_B}{Z_A}) & \frac{1}{2}(1 + \frac{Z_B}{Z_A}) \end{bmatrix}, \quad (11)$$

$P_A$  and  $P_B$  are the propagation matrixes in uniformly straight waveguide as following matixes,

$$P_A = \begin{bmatrix} e^{j\beta_A l_A} & 0 \\ 0 & e^{-j\beta_A l_A} \end{bmatrix}, \quad P_B = \begin{bmatrix} e^{j\beta_B l_B} & 0 \\ 0 & e^{-j\beta_B l_B} \end{bmatrix} \quad (12)$$

Through the simplification of Eq. (10)-(12), we can obtain the matrix  $M = D_{AB} P_B D_{BA} P_A$ ,  $m_{11}$ ,  $m_{12}$ ,  $m_{21}$ ,  $m_{22}$  are the elements of matrix  $M$  as following formulas,

$$m_{11} = (1 + \frac{Z_A}{Z_B}) e^{j(\beta_A l_A - \beta_B l_B)}, \quad (13)$$

$$m_{12} = (1 - \frac{Z_A}{Z_B}) e^{j(\beta_A l_A + \beta_B l_B)}, \quad (14)$$

$$m_{21} = (1 - \frac{Z_A}{Z_B}) e^{j(\beta_A l_A - \beta_B l_B)}, \quad (15)$$

$$m_{22} = (1 + \frac{Z_A}{Z_B}) e^{j(\beta_A l_A - \beta_B l_B)}. \quad (16)$$

Therefore, the transmittance  $T$  can be expressed as,

$$T = \left( \frac{1}{m_{11}} \right)^2 = \left( \frac{Z_B}{Z_A + Z_B} \right)^2. \quad (17)$$

The metal waveguide structure with grooves will generate the heat loss due to oscillation and collision free electron, and the terminus of the groove waveguide reflection will give a phase change. The characteristic impedance of groove  $B$  for the electric field can be obtained as,

$$Z_B = -jZ_A \cot\left(\frac{2\pi}{\lambda_{GP}} L\right). \quad (18)$$

Here,  $L$  is the length of the groove waveguide,  $L = 2l_A + l_B$ .  $\lambda_{GP}$  is the wavelength of the groove plasmon, and  $\lambda_{GP}$  satisfies,

$$\lambda_{GP} = \frac{\lambda}{real(n_{eff})}. \quad (19)$$

Considering the loss of metal waveguide, we can get the transmittance  $T$  from Port  $A_1$  to Port  $A_2$ ,

$$T = \frac{1}{1 + \tan^2(2\pi d_{B1}/\lambda_{GP})} \exp\left(-\frac{L}{L_{spp}}\right). \quad (20)$$

Here,  $L_{spp} = \frac{4\pi}{\lambda} \times \text{Im}(n_{eff})$ .

### III. SIMULATIONS AND RESULTS

The theory and simulation transmittance of the two symmetrical grooves waveguide structure is shown in Fig. 3(a). The length of the groove  $B$   $l_B$  is chosen to be  $0.05\mu\text{m}$ . The filtered wavelengths are nearly  $650\text{nm}$ ,  $715\text{nm}$ , and  $765\text{nm}$  with the selected depths of the grooves  $d_B = 0.10\mu\text{m}$ ,  $0.11\mu\text{m}$ , and  $0.12\mu\text{m}$ , respectively. While increasing  $d_B$ , the wavelengths which filtered out are enlarged as well. In addition, the transmittance increases with the increasing of the incident wavelength  $\lambda$  and tends to a constant value. The maximum transmittance at the wavelengths around  $2000\text{nm}$  is about  $80\%$ . The contour profiles of Magnetic field intensity distributions  $|H_y|^2$  of the symmetrical structures at different wavelengths with the grooves depths  $d_B = 0.10\mu\text{m}$  are shown in Fig. 3(b)-3(d). From Fig. 3(c), it can be observed that the transmission is  $0\%$  for  $\lambda = 650\text{nm}$ . In Fig. 3(b) and 3(d), for  $\lambda = 400\text{nm}$  and  $1550\text{nm}$ , the SPPs can propagate through the MIM wavelength structure and the

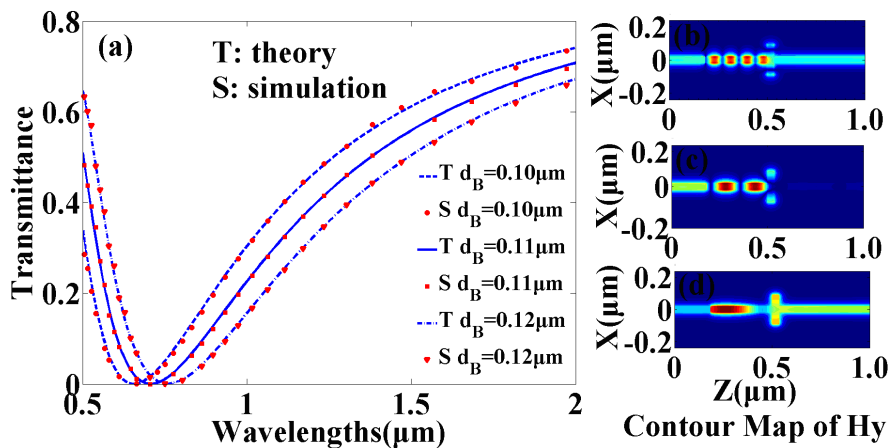


FIG. 3. (a) The transmittance of the symmetrical double-groove structure with  $d_B = 0.10\mu\text{m}$ ,  $0.11\mu\text{m}$ ,  $0.12\mu\text{m}$ , respectively. Wires and dots represent the theoretical and simulation data, respectively. Fig. 3(b) - (d) Magnetic field intensity distributions  $|H_y|^2$  of the grooves depths  $d_B = 0.10\mu\text{m}$  at different wavelengths (b)  $\lambda = 400\text{nm}$ , (c)  $650\text{nm}$ , (d)  $1550\text{nm}$ .

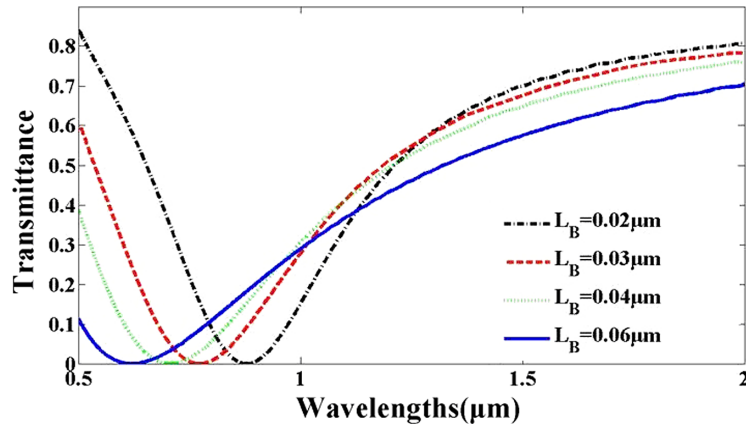


FIG. 4. The transmittance of the symmetrical double-groove structure with  $l_B = 0.02\mu\text{m}$ ,  $0.03\mu\text{m}$ ,  $0.04\mu\text{m}$  and  $0.06\mu\text{m}$ , respectively.

transmission increases with wavelength increasing. In our opinion, the symmetrical double-groove structure could serve as Fabry-Perot resonators and could be utilized as plasmonic pass or block filters. From the Fig. 3(a), we can get the simulation results are consistent with the theory results derived by the transmission line theory.

The transmittance of the symmetrical double-groove structure with different groove lengths is shown in figure 4. Here the depths of the groove  $B$   $d_B$  are chosen to be  $0.05\mu\text{m}$ , and the uniform lengths of the groove  $B$   $l_B$  are chosen to be  $0.02\mu\text{m}$ ,  $0.03\mu\text{m}$ ,  $0.04\mu\text{m}$ , and  $0.06\mu\text{m}$ , respectively. The filtered wavelengths are nearly  $877\text{nm}$ ,  $772\text{nm}$ ,  $705\text{nm}$  and  $621\text{nm}$  with the selected lengths of the grooves  $B$ . While decreasing  $l_B$ , the wavelengths which filtered out increase as well. According to Fig. 3 and Fig. 4, the symmetrical double-groove structures can achieve the filtering characteristics, and only one filtering wavelength can be achieved. The optical devices with definite filtered wavelength are achieved by changing the depths and lengths of the structure.

For the unsymmetrical double-groove structure, the transmission  $T$  investigated by using the transmission line theory can be obtained as

$$T = \frac{4}{4 + (\tan(2\pi d_1/\lambda_{GP}) + \tan((2\pi d_2/\lambda_{GP})))^2} \exp(-\frac{L}{L_{spp}}). \quad (21)$$

Here,  $\lambda_{GP} = \frac{\lambda}{real(n_{eff})}$ ,  $L_{spp} = \frac{4\pi}{\lambda} \times \text{Im}(n_{eff})$ .

To get more insights into the physics of the double-groove transmission observed, unsymmetrical double-groove structure is discussed, as in figure 5(a). The depths of grooves  $B_1$  and  $B_2$  are different, other parameters are same as shown in Fig. 2(a). Fig. 5(b) is the theory and simulation transmittance

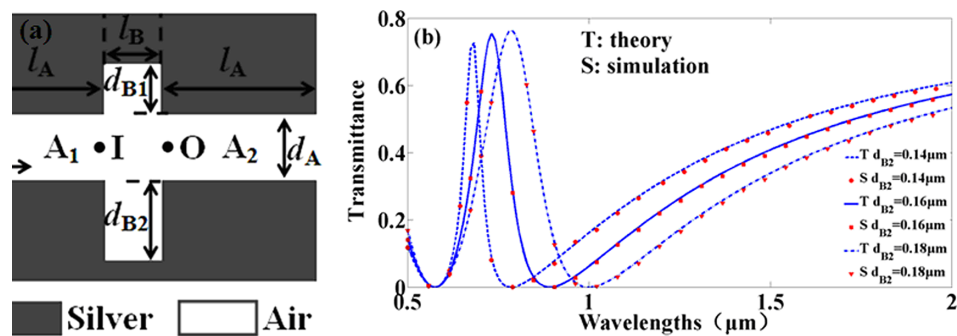


FIG. 5. (a) Schematic diagram of the unsymmetrical double-groove shaped plasmonic waveguide optical filters. (b) Transmission spectra of the different depths of the double-groove.  $d_{B1}$  is fixed to be  $0.10\mu\text{m}$ ,  $d_{B2} = 0.14\mu\text{m}$ ,  $0.16\mu\text{m}$  and  $0.18\mu\text{m}$ , respectively. Wires and dots represent the theoretical and simulation data, respectively.

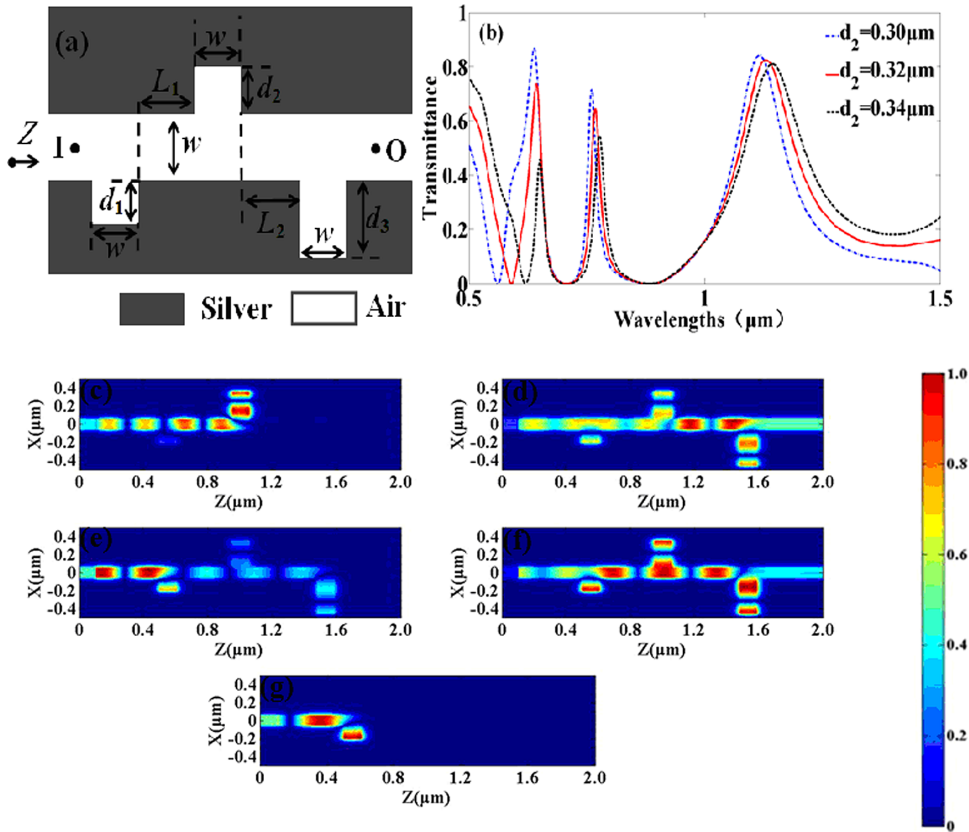


FIG. 6. (a) Schematic diagram of plasmonic waveguide coupled to three grooves. (b) The transmittance of the plasmonic waveguide coupled to three grooves. (c)-(g) Magnetic field intensity distributions  $|H_y|^2$  of the grooves depth  $d_2 = 0.30\mu\text{m}$  at different wavelengths of (c)  $\lambda = 560\text{nm}$ , (d)  $\lambda = 636\text{nm}$ , (e)  $\lambda = 707\text{nm}$ , (f)  $\lambda = 757\text{nm}$  and (g)  $\lambda = 883\text{nm}$ .

of the waveguide structure with unsymmetrical double-groove. Here, the depths of the groove  $B_2 d_{B1}$  is fixed to  $0.10\mu\text{m}$ , and the depths of the groove  $B_2 d_{B2}$  are chosen to be  $0.14\mu\text{m}, 0.16\mu\text{m}, 0.18\mu\text{m}$ , respectively. It is observed that there is a transmission peak for  $d_{B1} \neq d_{B2}$ . While increasing  $d_{B2}$ , the wavelength peak shifts to long wavelength ranges, and the half-maximum at full-widths increase from  $0.05\mu\text{m}$  to  $0.15\mu\text{m}$ . Obviously, this transmission peak is the electromagnetically induced transparency window. The transparency window are  $682\text{nm}, 731\text{nm}$  and  $780\text{nm}$  for  $d_{B2} = 0.14\mu\text{m}, 0.16\mu\text{m}$  and  $0.18\mu\text{m}$  in Fig. 5(b), respectively. The electromagnetically induced transparency is based on the destructive interference of the transition probability amplitude between atomic states. While increasing  $d_{B2}$ , the detuning extent is decreased and the half-maximum at full-widths become larger.

The figure 6(a) shows unsymmetrical third-groove structure. The dark component represents Ag and light component represents air. Here, the width of the groove and gap  $w$  is closed to be  $0.10\mu\text{m}$ .  $d_1, d_2$  and  $d_3$  are the depths of the three grooves, respectively.  $d_1, d_3$  are fixed to be  $0.15\mu\text{m}, 0.40\mu\text{m}$ , respectively, and  $d_2$  is variable. The lengths of two grooves  $L_1$  and  $L_2$  are  $0.25\mu\text{m}, 0.33\mu\text{m}$ , respectively. The transmittance of the plasmonic waveguide coupled to three grooves is shown in Fig. 6(b). The depths of the groove  $d_2$  are chosen to  $0.30\mu\text{m}, 0.32\mu\text{m}$ , and  $0.34\mu\text{m}$ , respectively. We can find three transmission valleys, correspond to different  $d_2$ , which transmittance is nearly 0%. For  $d_2$  is  $0.30\mu\text{m}$ , the transmission valleys are  $560\text{nm}, 707\text{nm}$ , and  $883\text{nm}$ , respectively. The contour profiles of Magnetic field intensity distributions  $|H_y|^2$  with the grooves depth  $d_2 = 0.30\mu\text{m}$  are shown in Fig. 6(c)-(g). From Fig. 6(c), it can be observed that the transmission is 0% for  $\lambda = 560\text{nm}$ , and the field distributions  $|H_y|^2$  vanish at the second groove. Similarly, the other two transmission valleys are  $707\text{nm}$  and  $883\text{nm}$ , shown in Fig. 6(e) and (g), the field distributions  $|H_y|^2$  disappear at the third groove and first groove, respectively. For the transmission peaks  $\lambda = 636\text{nm}$  and  $757\text{nm}$ , as the Fig. 6(d) and (f), the SPPs can propagate through this structure.

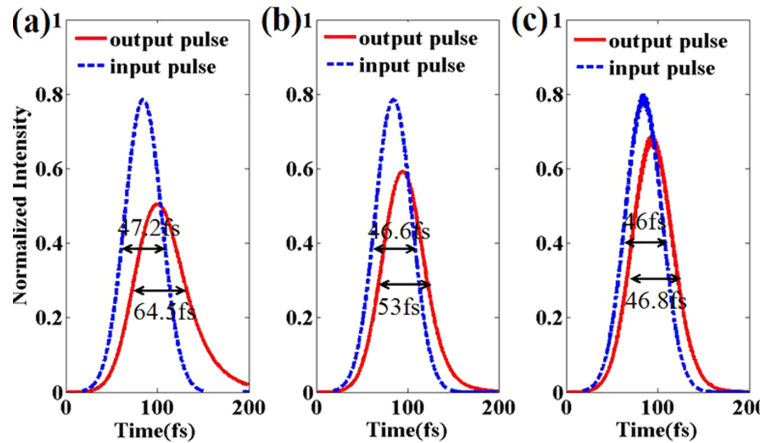


FIG. 7. Time evolution of intensity profile of the SPP pulse propagating through the plasmonic waveguide structure with the depth of upwards groove  $d_1 = 0.10\mu\text{m}$ . (a) the depth of the downwards groove  $d_2 = 0.12\mu\text{m}$ , (b) the depth of the downwards groove  $d_2 = 0.13\mu\text{m}$ , (c) the depth of the downwards groove  $d_2 = 0.14\mu\text{m}$ .

The electromagnetically induced transparency window can be chosen to study the expected phenomenon of slow-SPPs propagation. To analysis the phenomenon of slow SPPs, we investigate the time evolution of the pulse propagating through the plasmonic waveguide with unsymmetrical double-groove structure. Fig. 7 is the time evolution of intensity profile of the SPP pulse propagating through the plasmonic waveguide with different depths of the downwards groove. Here, the depths of the upwards groove  $d_{B1}$  is fixed to  $0.10\mu\text{m}$ , and the depths of the downwards groove  $d_{B2}$  is  $0.12\mu\text{m}$ ,  $0.13\mu\text{m}$ ,  $0.14\mu\text{m}$ , respectively. We put two observation points in points  $I$  and  $O$  to record the pulse time evolution, and points  $I$  and  $O$  are located in the output and input planes of the unsymmetrical double-groove structure shown in Fig. 5(a).  $\tau$  is the optical delay time, which is calculated by the peak difference between the output pulse and input pulse. Dashed lines represent the input pulse, and solid lines represent the output pulse shown in Fig. 7. The group index  $n_g$  is expressed by  $n_g = c/v_g$ . Here,  $v_g$  stands for the group velocity in the plasmonic waveguide systems.  $v_g$  can be calculated using  $D/\tau$ .  $D$  is the propagating distance of plasmonic mode between  $O$  and  $I$ , so  $D$  is equal to the width of groove  $w = 0.05\mu\text{m}$ . The wavelengths of the incident light are  $830\text{nm}$ ,  $855\text{nm}$ ,  $870\text{nm}$ , respectively, which are corresponding to the transparency windows. In Fig. 7(a), the  $830\text{nm}$  of the transparency peak ( $d_{B1} = 0.10\mu\text{m}$ ,  $d_{B2} = 0.12\mu\text{m}$ ) is chosen as the working wavelength, the delay time is  $13.5\text{fs}$ , and  $n_g = 81$  is obtained. The half-maximum at full-width of the incident pulse in the plasmonic waveguide structure is  $47.2\text{fs}$ , while that of output pulse is  $64.5\text{fs}$ . The relative pulse shape distortion is  $36.7\%$ . In Fig. 7(b), the  $855\text{nm}$  of the transparency peak ( $d_{B1} = 0.10\mu\text{m}$ ,  $d_{B2} = 0.13\mu\text{m}$ ) is chosen as the working wavelength, the delay time is  $8\text{fs}$ , and  $n_g = 48$  is obtained. The half-maximum at full-width of the incident pulse in the MIM plasmonic waveguide structure is  $46.6\text{fs}$ , while the output pulse is  $53\text{fs}$ . The relative pulse shape distortion is  $13.7\%$ . In Fig. 7(c), the  $875\text{nm}$  of the transparency peak ( $d_{B1} = 0.10\mu\text{m}$ ,  $d_{B2} = 0.14\mu\text{m}$ ) is chosen as the working wavelength, the delay time is  $6\text{fs}$ , and  $n_g = 36$  is obtained. The half-maximum at full-width of the incident pulse in the plasmonic waveguide structure is  $46\text{fs}$ , while that of output pulse is  $46.8\text{fs}$ . The relative pulse shape distortion is only  $1.74\%$ .

Similarly, Fig. 8 is the time evolution of intensity profile of the SPP pulse propagating through the unsymmetrical third-groove structure with depths of the groove  $d_1 = 0.15\mu\text{m}$ ,  $d_2 = 0.30\mu\text{m}$ ,  $d_3 = 0.40\mu\text{m}$ . We put two observation points in points  $I$  and  $O$  to record the pulse time evolution, and points  $I$  and  $O$  are located in the output and input planes of the third-groove shown in Fig. 6(a).  $\tau$  is the optical delay time, which is calculated by the peak difference between the output pulse and input pulse. Solid lines represent the input pulse, and dashed lines represent the output pulse in Fig. 8. Here  $D$  is equal to the width of groove of unsymmetrical third-groove structure  $w = 0.1\mu\text{m}$ . The wavelengths of the incident light are  $636\text{nm}$ ,  $757\text{nm}$  shown in Fig. 8(a)-(b), respectively, which are corresponding to the transparency windows. In Fig. 8(a), the  $636\text{nm}$  of the transparency peak

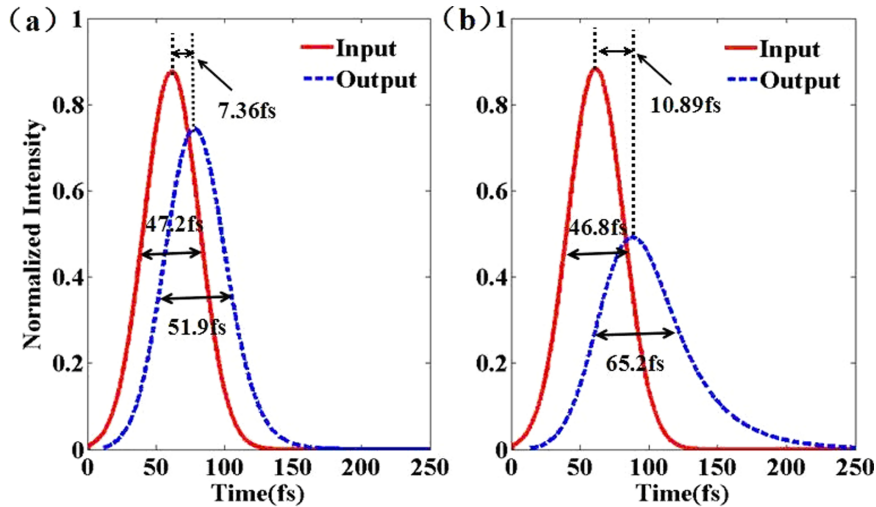


FIG. 8. Time evolution of intensity profile of the SPP pulse propagating through the unsymmetrical third-groove structure (a)  $\lambda = 636\text{nm}$  (b)  $\lambda = 757\text{nm}$ .

is chosen as the working wavelength, the delay time is 7.36fs, and  $n_g = 7.95$  is obtained. The half-maximum at full-width of the incident pulse in the plasmonic waveguide structure is 47.2fs, while the output pulse is 51.9fs. The relative pulse shape distortion is 9.96%. In Fig. 8(b), the 757nm of the transparency peak is chosen as the working wavelength, the delay time is 10.89fs, and  $n_g = 11.7$  is obtained. The half-maximum at full-width of the incident pulse in the plasmonic waveguide structure is 46.8fs, while that of output pulse is 65.2fs. The relative pulse shape distortion is 39.3%. In fact, the real group index  $n_g$  of the groove is greater than the group index  $n_g$  that we calculated. The plasmonic waveguide coupled to three grooves is proposed significant applications in slow-light systems, especially optical buffers. We can conclude that the distortion will become larger with the increase of  $n_g$ , which restricts the applicability of these structures.

The group index  $n_g$  and  $\delta_t$  vs the transparency peaks  $\lambda_0$  of unsymmetrical double-groove structure is plotted in Fig. 9. Here, the transparency peaks  $\lambda_0$  are corresponding to the transparency

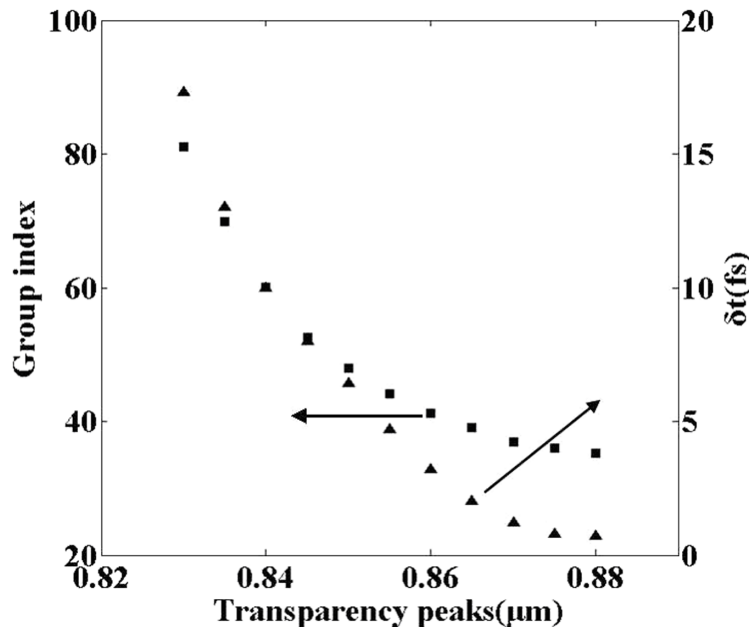


FIG. 9. The group index  $n_g$  (squares) and  $\delta_t$  (triangles) vs the transparency peaks  $\lambda_0$  of unsymmetrical double-groove structure.

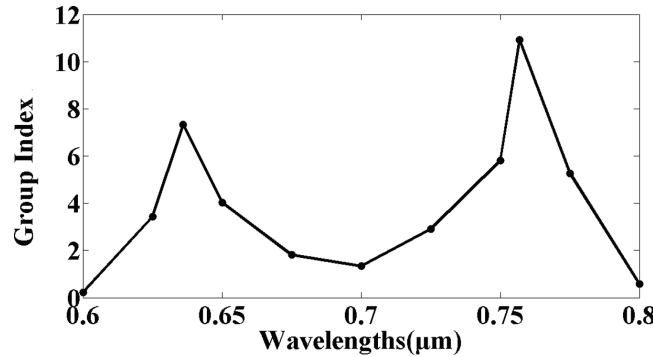


FIG. 10. The group index  $n_g$  (squares) vs the wavelength  $\lambda_0$  unsymmetrical third-groove structure.

windows for the different depths of the downwards groove  $d_{B2}$ . From the relationship between  $n_g$  and  $\lambda_0$ , we can find that  $n_g$  decreases from 81 to 35 with the increasing of  $\lambda_0$  from 830nm to 880nm.  $\delta_t$  is the difference between the half-maximum at full-widths of the input and output pulse, and it demonstrates the distortion of the plasmonic mode. Fig. 9 shows that the relationship between  $\delta_t$  and  $\lambda_0$  is as the same as the relationship between  $n_g$  and  $\lambda_0$ , and  $\delta_t$  decreases from 17fs to 0.7fs. In addition, the group index  $n_g$  versus the transparency peaks  $\lambda_0$  of unsymmetrical third-groove structure is plotted in Fig. 10. Here, the transparency peaks  $\lambda_0$  are corresponding to the transparency windows for the depth of groove  $d_2 = 0.30\mu\text{m}$ . From the relationship between  $n_g$  and  $\lambda_0$ , we can find the local maximum values of  $n_g$  when  $\lambda_0 = 636\text{nm}$  and  $757\text{nm}$ , the results coincided with the Fig. 8. Fig. 10 demonstrates the distortion of the plasmonic mode. Thus, there is a trade-off between the group index  $n_g$  and the distortion for the plasmonic mode in such slow-light effect waveguide structure. EIT phenomenon need following conditions: interference between the two resonant modes with different characteristics. One resonance mode is excited by external fields and lead to energy absorption more easily, which is the so-called bright state (bright mode). Another resonance mode cannot be directly excited by the external fields, which is the so-called black state (dark mode). When the two resonance modes are coupling in a system, the bright mode is excited at first, the dark mode is shown by the coupling effects between the two patterns. The interaction between the two models makes the bright state absorption spectrum to split into two absorption spectra. Thus, it is emerged a high-transparency window between two absorption spectra.

#### IV. CONCLUSIONS

In summary, the novel MIM plasmonic waveguide filters with unsymmetrical grooves are investigated. This metallic waveguide structures show filtering characteristics. We have numerically described that the unsymmetrical grooves in the plasmonic waveguide structures play significant role in developing wavelength selective filters of subwavelength sizes. The transmittance formulas are deduced by transmission line theory. Our results suggest that the transmission are related to geometrical parameters of the groove structures. When the effects of the unsymmetrical grooves are detuned, we can observe plasmonic induced transparency and slow light effects. PIT and slow light effects can be used to construct the sensor with high sensitivity, for example, fiber optic delay, optical buffer, and optical communication devices.

#### ACKNOWLEDGMENT

This work is supported by the NSFC under Grant No. 11347196, the Natural Science Foundation of Jiangsu Province of China under Grant No. BK20140167, BK20140128, BK2012548, the Fundamental Research Funds for the Central Universities of China under Grant No. JUSRP211A20, and the National Training Programs of Innovation and Entrepreneurship for Undergraduates under Grant No. 201410295027.

- <sup>1</sup> P. Berini, *Phys. Rev. B* **61**, 10484–10503 (2000).
- <sup>2</sup> W. L. Barnes, A. Dereux, and T. W. Ebbesen, *Nature* **424**, 824–830 (2003).
- <sup>3</sup> D. K. Gramotnev and S. I. Bozhevolnyi, *Nat. Photonics* **4**, 83–91 (2010).
- <sup>4</sup> W. Nomura, M. Ohtsu, and T. Yatsui, *Appl. Phys. Lett.* **86**, 181108 (2005).
- <sup>5</sup> G. Veronis and S. Fan, *Appl. Phys. Lett.* **87**, 131102 (2005).
- <sup>6</sup> T. Lee and S. Gray, *Opt. Express* **13**, 9652–9659 (2005).
- <sup>7</sup> H. Gao, H. Shi, C. Wang, C. Du, X. Luo, Q. Deng, Y. Lv, X. Lin, and H. Yao, *Opt. Express* **13**, 10795–10800 (2005).
- <sup>8</sup> H. Zhao, X. Huang, and J. Huang, *Physica E* **40**, 3025–3029 (2008).
- <sup>9</sup> Z. Han and S. He, *Opt. Commun.* **278**, 199–203 (2007).
- <sup>10</sup> Z. Han, L. Liu, and E. Forsberg, *Opt. Commun.* **259**, 690–695 (2006).
- <sup>11</sup> H. Lu, X. Liu, Y. Gong, D. Mao, and L. Wang, *Opt. Express* **19**, 12885–12890 (2011).
- <sup>12</sup> Y. Gong, L. Wang, X. Liu, and X. Li, *Opt. Express* **17**, 13727–13736 (2009).
- <sup>13</sup> Q. Q. Gan, B. S. Guo, G. F. Song, L. H. Chen, Z. Fu, Y. J. Ding, and F. J. Bartoli, *Appl. Phys. Lett.* **90**, 161130 (2007).
- <sup>14</sup> Q. Q. Gan, Z. Fu, Y. J. Ding, and F. J. Bartoli, *Opt. Express* **15**, 18050–18055 (2007).
- <sup>15</sup> Z. Fu, Q. Gan, K. Gao, Z. Pan, and F. J. Bartoli, *J. Lightwave Technol.* **26**, 3699–3703 (2008).
- <sup>16</sup> N. Bonod, E. Popov, L. Li, and B. Chernov, *Optics Express* **15**, 11427–11432 (2007).
- <sup>17</sup> F. L. Tejeira, S. G. Rodrigo, L. M. Moreno, F. J. G. Vidal, E. Devaux, T. W. Ebbesen, J. R. Krenn, I. P. Radko, S. I. Bozhevolnyi, M. U. Gonzalez, J. C. Weeber, and A. Dereux, *Nat. Phys.* **3**, 324–328 (2007).
- <sup>18</sup> T. F. Krauss, *Nat. Photonics* **2**, 448–450 (2008).
- <sup>19</sup> C. Liu, Z. Dutton, C. Behroozi, and L. Hau, *Nature* **409**, 409–411 (2001).
- <sup>20</sup> J. B. Khurgin, *J. Opt. Soc. Am. B* **22**, 1062–1074 (2005).
- <sup>21</sup> M. T. Hill, H. J. S. Dorren, T. De Vries, X. J. M. Leijtens, J. H. D. Besten, B. Smalbrugge, Y. S. Oei, H. Binsma, G. D. Khoe, and M. K. Smit, *Nature* **432**, 206–209 (2004).
- <sup>22</sup> F. Xia, L. Sekaric, and Y. Vlasov, *Nat. Photonics* **1**, 65–71 (2007).
- <sup>23</sup> K. -J. Boller, A. Imamolu, and S. Harris, *Phys. Rev. Lett.* **66**, 2593–2596 (1991).
- <sup>24</sup> M. Fleischhauer, A. Imamoglu, and J. P. Marangos, *Rev. Mod. Phys.* **77**, 633–673 (2005).
- <sup>25</sup> S. Darmawan, L. Y. M. Tobing, and D. H. Zhang, *Opt. Express* **19**, 17813–17819 (2011).
- <sup>26</sup> F. G. Liu, M. Z. Ke, A. Q. Zhang, W. J. Wen, J. Shi, Z. Y. Liu, and P. Sheng, *Phys. Rev. E* **82**, 026601 (2010).
- <sup>27</sup> R. D. Kekatpure, E. S. Barnard, W. Cai, and M. L. Brongersma, *Phys. Rev. Lett.* **104**, 243902 (2010).
- <sup>28</sup> Y. K. Wang, J. C. Wang, C. Liu, Q. Luo, W. X. Zhang, and S. M. Gao, *Appl. Phys. Express* **6**, 082201 (2013).
- <sup>29</sup> Y. Huang, C. Min, and G. Veronis, *Appl. Phys. Lett.* **99**, 43117–43119 (2011).
- <sup>30</sup> Z. Han and S. I. Bozhevolnyi, *Opt. Express* **19**, 3251–3257 (2011).
- <sup>31</sup> J. J. Chen, C. Wang, R. Zhang, and J. H. Xiao, *Opt. Lett.* **37**, 5133–5135 (2012).
- <sup>32</sup> J. J. Chen, Z. Li, S. Yue, J. H. Xiao, and Q. H. Gong, *Nano Lett.* **12**, 2494–2498 (2012).
- <sup>33</sup> S. Biswas, J. S. Duan, D. Nepal, K. Park, R. Pachter, and R. A. Vaia, *Nano Lett.* **13**, 6287–6291 (2013).
- <sup>34</sup> J. Song, J. Liu, K. Li, Y. Song, X. Wei, and G. Song, *IEEE Photonics Technol. Lett.* **26**, 1104–1107 (2014).
- <sup>35</sup> M. Miyata, J. Hirohata, Y. Nagasaki, and J. Takahara, *Opt. Express* **22**, 11399–11406 (2014).
- <sup>36</sup> X. Yang, X. Hu, Z. Chai, C. Lu, H. Yang, and Q. H. Gong, *Appl. Phys. Lett.* **104**, 221114 (2014).
- <sup>37</sup> B. Yun, G. Hu, C. Wei, and Y. Cui, *Mater. Res. Express* **1**, 036201 (2014).
- <sup>38</sup> H. Lu, X. Liu, D. Mao, Y. Gong, and G. Wang, *Opt. Lett.* **36**, 3233 (2011).